Article

Evolution of Turbulence in the Kelvin–Helmholtz Instability in the Terrestrial Magnetopause

Francesca Di Mare [1,*], **Luca Sorriso-Valvo** [2,3] (iD), **Alessandro Retinò** [4], **Francesco Malara** [5] (iD) and **Hiroshi Hasegawa** [6] (iD)

1   Department of Physics, University of Oslo, 1048 Blindern, 0316 Oslo, Norway
2   Departamento de Física, Escuela Politécnica Nacional, Av. Ladrón de Guevara E11–253, 170517 Quito, Ecuador; lucasorriso@gmail.com
3   ISTP/CNR, U.O.S. di Bari, Via Amendola, 122/D 70126 Bari, Italy
4   Laboratoire de Physique des Plasmas, CNRS/Ecole Polytechnique/Sorbonne Université/Université Paris Sud/Observatoire de Paris, route de Saclay, F-91128 Palaiseau, France; alessandro.retino@lpp.polytechnique.fr
5   Dipartimento di Fisica, Università della Calabria, Ponte P. Bucci, cubo 31C, 87036 Rende, Italy; francesco.malara@fis.unical.it
6   Institute of Space and Aeronautical Science, JAXA, 3-1-1 Yoshinodai, Chuo, Sagamihara, Kanagawa 252-5210, Japan; hase@stp.isas.jaxa.jp
*   Correspondence: f.d.mare@fys.uio.no

Abstract: The dynamics occurring at the terrestrial magnetopause are investigated by using Geotail and THEMIS spacecraft data of magnetopause crossings during ongoing Kelvin–Helmholtz instability. Properties of plasma turbulence and intermittency are presented, with the aim of understanding the evolution of the turbulence as a result of the development of Kelvin–Helmholtz instability. The data have been tested against standard diagnostics for intermittent turbulence, such as the autocorrelation function, the spectral analysis and the scale-dependent statistics of the magnetic field increments. A quasi-periodic modulation of different scaling exponents may exist along the direction of propagation of the Kelvin–Helmholtz waves along the Geocentric Solar Magnetosphere coordinate system (GSM), and it is visible as a quasi-periodic modulation of the scaling exponents we have studied. The wave period associated with such oscillation was estimated to be approximately 6.4 Earth Radii (R_E). Furthermore, the amplitude of such modulation seems to decrease as the measurements are taken further away from the Earth along the magnetopause, in particular after $X(GSM) \lesssim -15\ R_E$. The observed modulation seems to persist for most of the parameters considered in this analysis. This suggests that a kind of signature related to the development of the Kelvin–Helmholtz instabilities could be present in the statistical properties of the magnetic turbulence.

Keywords: magnetosheath; Kelvin–Helmholtz instability; turbulence; intermittency

1. Introduction

Turbulence at the interface between the solar wind and the magnetosphere is an important subject in space physics. Properties of turbulence can help with understanding the transport of mass, momentum, and energy from the solar wind to the magnetosphere [1,2] and, more generally, the mechanisms of interaction between these two regions of the near-Earth space.

The Kelvin–Helmholtz Instability (KHI) can drive waves at the magnetopause. These waves can grow to form rolled-up vortices and facilitate transfer of plasma into the magnetosphere. This mechanism is considered one of the most important in the low-latitude boundary layer (LLBL) during

periods of northward Interplanetary Magnetic Field (IMF) [3], when reconnection at the equatorial magnetopause is less effective [4,5]. The Kelvin–Helmholtz instability can grow at the low-latitude magnetopause, situated between the magnetosheath, characterized by an anti-sunward flow of shocked solar wind, and the outer plasma sheet characterized by stagnant or weak sunward flows [6]. When the IMF is northward, the equatorial component of the magnetic field can be negligible at low latitude and so the KHI can develop eventually producing fully rolled-up vortices. There is an extensive literature for understanding development of this instability along the inner edge of the LLBL [7,8]. The resulting waves or vortices are suggested to have some relation to aurorae with spatially periodic forms [9,10]. There are observational evidence of the KHI in the form of surface waves propagating anti-sunward along the magnetopause [7,11–13]. A shared point of view considers Kelvin–Helmholtz waves or vortices to be more frequent during northward IMF conditions than during southward IMF [13–15]. Those vortices are believed to be a key ingredient for the formation of the thick LLBL [3] and of the cold and dense plasma sheet (CDPS) [16,17], both encountered predominantly under northward IMF. Kelvin–Helmholtz waves are known to develop at a planetary magnetopause, where small scale perturbations gain energy from the velocity shear between the magnetospheric and magnetosheath plasma and thereby grow into large scale rolled up vortices [18]. When the waves reach a turbulent state, plasma and energy are transported from the dense magnetosheath into the more rarified magnetosphere [19]. There is a lot of observational evidence to demonstrate the presence of Kelvin–Helmholtz waves on both the dawn and dusk flank of the terrestrial magnetosphere spanning approximately from the dawn–dusk meridian to 30 Earth radii down the magnetotail [12,14,20–25]. It looks like that the events arise in the proximity of the equatorial plane, where the magnetopause is believed to be susceptible to the KHI [23,26].

The KHI can also drive the turbulence in the magnetosheath region [11,12,21,23–25,27]. It is therefore interesting to study the characteristics of turbulence in the KHI regions, trying to understand the relationship between the instability and the various characteristics of turbulence such as power-law spectra and intermittency. To this aim, we analyzed the statistical properties of turbulence from a collection of Geotail observations, spanning nine years from 1995 to 2003. These events have been previously selected and studied by Fairfield et al. [12], Hasegawa et al. [15], Fujimoto et al. [28], Stenuit et al. [29]. To enrich the dataset, two additional events from THEMIS observations during November 2008, previously studied by Lin et al. [30], have been investigated. All events are encountered along the flank magnetopause, most of which are behind the dawn–dusk terminator, showing quasi-periodic plasma and field fluctuations in the flank low-latitude boundary layer under northward IMF, associated with Kelvin–Helmholtz waves. In Section 2, we present the dataset used for the analysis; in Section 3, we analyse the properties of turbulence, such as the autocorrelation function, the spectrum and the scale-dependent statistics of the field increments; in Section 4, we study the evolution of turbulence along the KHI; finally, in Section 5, we comment on the results obtained.

2. The Data: Geotail and THEMIS Magnetopause Crossing

The description of the properties of turbulence is customarily performed through the high-order statistical analysis of the field increments. This requires that each interval should have a statistically significant number of measurements. As a rule of thumb, the correct estimate of the qth order moment requires $\gtrsim 10^q$ measurements in order to ensure convergence. Based on this, in order to enable the computation of the fourth-order moments, we have selected a set of intervals each including a number of data points $N \gtrsim 10^4$. Furthermore, we used intervals that are not affected by an excessive presence of data gaps, so that missing points are less than 10%. According to these requirements, we have selected 17 Geotail events from the list of 19 reported by Hasegawa et al. [15]. Only two THEMIS events from the set of 14 reported by Lin et al. [30] have been chosen as the only ones with an interesting position for our analysis, i.e., behind the dawn–dusk terminator on the left-side where we have fewer Geotail events. The observed condition of all events are listed in Table 1 and in Table A1 in Appendix A. Table 1 shows the following information (from Hasegawa et al. [15]): date; time interval; GSM position

measured in units of the Earth radius R_E; IMF condition; ion mixing status; fluctuation period, related to the rolled-up vortices; magnetosheath mean bulk velocity v_{ms}; wavelength λ, obtained multiplying the magnetosheath flow speed by the fluctuation period, and dividing by 1 R_E. The ion mixing status is defined "mixed" if a significant amount of cool magnetosheath-like ions was present on the magnetospheric side of the magnetopause, where the density, evaluated using the full phase space distribution, is $n > 1/\text{cm}^3$; or "weakly-mixed", when magnetosheath-like ions were found on magnetospheric side, with density lower than $n < 1/\text{cm}^3$. The fluctuation period corresponds to the perturbations in the flow that are interpreted by Hasegawa et al. [15] as being due to vortical motions of plasma (e.g., Fujimoto et al. [14]), whereas those in the magnetic field are due to deformation of the field lines when those near the magnetopause are brought into rolled-up vortices [23,31]. The event recorded on 25 March 2002 (event F) is split into two different sets F_a and F_b because it presents a large gap in its central part.

Table 1. Event List of rolled-up vortices detected by Geotail over nine years from 1995 to 2003, adapted from Hasegawa et al. [15]. The last two events were detected by THEMIS probe C, adapted by Lin et al. [30].

Event	Interval	GSM Position	IMF Condition	Mixing Status	Period	v_{ms}	λ
GEOTAIL MISSION							
S	1995-03-24 0600-0800	$(-15, 20, 4)$	ES[1] NBZ[2]	Mixed	2–3	227	5.3
O	1997-01-10 2050-2400	$(-7, 16, 4)$	ND[3] NBZ after N-t[4]	Weakly mixed	2–3	169	4.0
P	1997-01-11 0400-0500	$(-13, 16, 4)$	ES NBZ	Mixed	~ 3	219	6.2
Q	1997-02-12 1430-1600	$(-13, 22, 3)$	ES NBZ	Mixed	~ 2	281	5.3
T	1998-04-13 0315-0430	$(-18, 20, 4)$	ES NBZ	Mixed	2–3	312	7.3
L	1998-08-01 0530-0730	$(0, 14, -3)$	ES NBZ	Mixed	~ 3	92	2.6
D	1998-12-27 1800-2100	$(-21, -22, -4)$	ES NBZ	Mixed	3–4	247	8.1
N	1999-02-15 1445-1515	$(-4, 16, 2)$	NBZ after N-t	Mixed	~ 2	279	5.3
M	1999-07-20 0630-0730	$(-3, 16, -2)$	ES NBZ	Mixed	2–3	230	5.4
E	2000-11-01 1030-1200	$(-8, -16, 6)$	ES NBZ	Mixed	2-3	298	7.0
H	2001-01-25 1330-1630	$(-22, -21, 0)$	ES NBZ	Mixed	~ 5	182	8.6
B	2001-11-16 1900-2000	$(-7, -18, 2)$	Extended NBZ (often ND)	Weakly mixed	2–3	183	4.3
C	2001-12-07 2000-2130	$(-11, -19, -1)$	SNBZ[5] after N-t	Weakly mixed	~ 3	257	7.3
E2	2002-03-25 0530-0900	$(-12, -17, -2)$	ES NBZ	Mixed	2–3	299	7.0
F	2002-03-25 1000-1300	$(-8, -16, -1)$	ES NBZ	Mixed	2–3	299, 347	7.0, 8.2
A	2002-10-15 2100-2300	$(-1, -14, 3)$	Extended NBZ	Mixed	2–3	332	7.8
R	2003-07-17 0330-0500	$(-13, 23, -1)$	ND NBZ after N-t	Weakly mixed	~ 2	419	7.9
THEMIS MISSION							
TH1	2008-11-06 0850-0920	$(-0.3, -15.3, 4.6)$	ES NBZ	Mixed	~ 2	288	3.3
TH2	2008-11-18 0720-0730	$(-2.3, -17, 3.4)$	ES NBZ	Mixed	~ 3	348	3.5

ES^1: extended strong; NBZ^2: northward IMF; ND^3: non dominant; $N - t^4$: N-turning; $SNBZ^5$: strong NBZ; Mixed/Weakly mixed means that a significant/small amount of magnetosheath ions was identified, i.e., n>/</1/cm^3, in the BL.

The locations of all the selected events are presented in Figure 1. As can be seen, most of the events are behind the dawn–dusk terminator, and, more precisely: nine on the dawn-side (left-side in Figure 1) and nine on the dusk-side (right-side in Figure 1). Events E and E2 present the same X and Y (GSM) coordinates, so they are over-plotted on top of each other. From now on, we refer to the GSM coordinates with X, Y and Z in capital letters and for the magnetic field component in the same direction with x, y, z in lower case letters. Before proceeding to the analysis of the turbulence properties of the data, it is necessary to test the validity of the Taylor hypothesis, which allows the switch between time and space measurements [32]. In particular, the time series of a field can be assumed to be an instantaneous spatial scan of the field if the typical velocities associated with the dynamics are slower than the probe speed inside the medium. To be more precise, for a turbulent distribution of modes in wavevector space, the plasma-frame frequency term ω and spatial advection term $\mathbf{k} \cdot \mathbf{v_{ms}}$, (where $\mathbf{v}_{ms}$

is the mean speed of each sample and the subscript "ms" indicates "magnetosheath" region, where our dataset is located), both contribute to the spacecraft-frame frequency [33], according to the relation [32]:

$$\omega_{sc} = \omega + \mathbf{k} \cdot \mathbf{v_{ms}}. \tag{1}$$
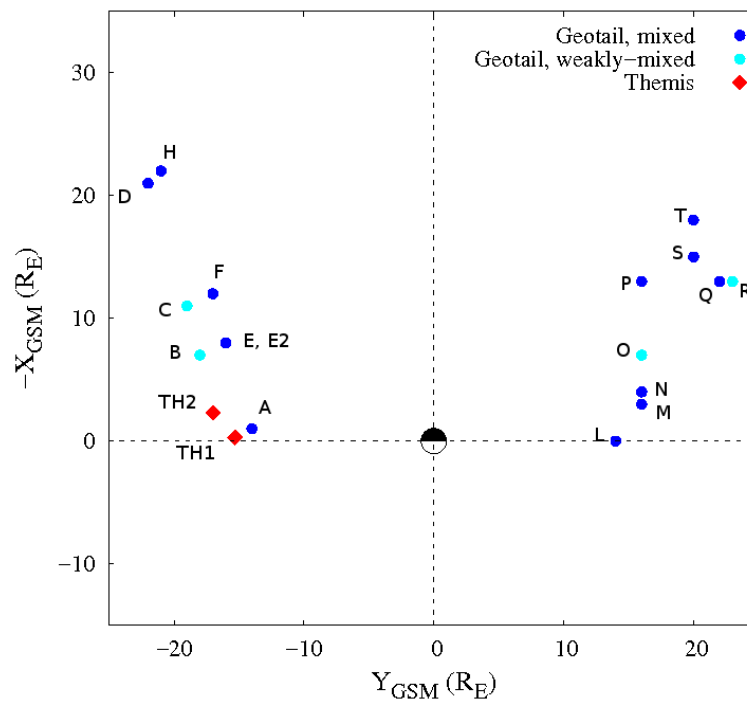

Figure 1. Locations of rolled-up Kelvin–Helmholtz events identified from Geotail (light-blue/blue dot) and THEMIS (red diamond).

As stated above, assuming $\omega \sim kv_A$, and for a super-Alfvénic flow, $v_{ms} \gg v_A$, then Equation (1) would imply $\omega_{sc} \simeq \mathbf{k} \cdot \mathbf{v}_{ms}$, thereby relating the spacecraft-frame frequency directly to the wavenumber of spatial fluctuations. This would correspond to the Taylor hypothesis [32,34].

In order to test the validity of the Taylor hypothesis in the samples studied here, values of the magnetosheath mean bulk speed and of the Alfvén speed were estimated for each interval under study. Unfortunately, their values are of the same order for almost all of the samples, so that the Taylor hypothesis does not hold, as shown in Table 2. However, it is possible to invoke a phenomenological approximation as an alternative to the Taylor hypothesis, previously presented by Stawarz et al. [35], and utilized in other magnetospheric studies of turbulence [36,37]. These authors assume that fluctuations are mainly Alfvénic (at least in the large-scale domain), so that their frequency in the plasma frame can be estimated as $\omega \sim \mathbf{k} \cdot \mathbf{v}_A = kv_A \cos\theta$, where θ is the angle between $\mathbf{k}$ and $\mathbf{B}_0$. Indicating by ϕ the angle between $\mathbf{k}$ and $\mathbf{v}_{ms}$, the advection term is $\mathbf{k} \cdot \mathbf{v}_{ms} = kv_{ms} \cos\phi$. Since in our samples $v_{ms} \sim v_A$, the advection term dominates over the frequency term (thus allowing space-time conversion in the time series) only when $\cos\theta \ll \cos\phi$, it is well known that, in magnetohydrodynamic (MHD) turbulence, the energy cascade tends to develop in the directions perpendicular to the mean magnetic field $\mathbf{B}_0$, so that perpendicular wave-vectors $k_\perp$ dominate over parallel wave-vectors $k_{||}$. Thus, we can expect that θ is close to $\pi/2$. Examining our data, we verified that the mean magnetic field $\mathbf{B}_0$ is mainly oriented in the z-direction (in GSM coordinates), therefore $\mathbf{k}$ is essentially in the xy

plane. Instead, the plasma bulk velocity $\mathbf{v}_{ms}$ is in the x-direction, i.e., mainly perpendicular to $\mathbf{B}_0$. This is confirmed by calculating the angle α between $\mathbf{B}_0$ and $\mathbf{v}_{ms}$ as

$$\alpha = arccos\left(\frac{\mathbf{B_0} \cdot \mathbf{v_{ms}}}{|\mathbf{B_0}|\,|\mathbf{v_{ms}}|} \right) , \tag{2}$$

which is consistently close to $90°$ for all samples (Table 2). This implies that the condition $\cos\theta \ll \cos\phi$ is satisfied in our database, so that the argument given by Stawarz et al. [35] holds, and the time series can be interpreted in terms of spatial measurements.

Table 2. Values of the magnetosheath mean bulk velocity v_{ms}, the Alfvén speed v_A and the angle α between $\mathbf{B}_0$ and $\mathbf{v}_{ms}$ estimated for each interval.

	v_A (km/s)	v_{ms} (km/s)	α (deg)
A	547	332	104,34
B	315	183	80,83
C	345	257	117,32
D	204	247	68,41
E	268	298	99,1
E2	400	299	60,69
F	344	347	76,15
H	182	182	65,2
L	286	92	72,58
M	200	230	92,84
N	234	279	85,41
O	232	169	71,98
P	268	219	64,57
Q	181	281	90,8
R	260	419	110,54
S	173	227	99,84
T	456	312	55,97
TH1	219	288	72,76
TH2	307	348	139,23

For the present analysis, we used the magnetic field time series sampled at $dt = 0.0625$ s obtained by the ASCII listings of Geotail MGF (Magnetic Field Measurement) high resolution magnetic field data (1/16 s sampling), where we got the data of magnetic field. Instead, the ASCII listings of Geotail LEP ion moment data (12 s sampling) was adopted to get the data of density and plasma velocity. The official website http://themis.ssl.berkeley.edu provides THEMIS data. We have worked with magnetic field data by an FGM (flux gate magnetometer) instrument at high resolution (1/128 s sampling), density and plasma velocity data taken by MOM (on-board moments) instrument at low resolution (3 s sampling). The frame of reference is the Geocentric Solar Magnetospheric (GSM) that has its X-axis towards the Sun and its Z-axis is the projection of the Earth's magnetic dipole axis (positive North) on to the plane perpendicular to the X-axis. The direction of the geomagnetic field near the nose of the magnetosphere is well ordered by this system. Thus, it is considered the best system to study the effects of interplanetary magnetic field components (e.g., B_z) on magnetospheric and ionospheric phenomena (see Hapgood [38], Russell [39]).

3. Analysis

In order to characterize the properties of the fluctuations, any event was analyzed using the standard diagnostics for intermittent turbulence. For each event, we have obtained: the autocorrelation function, which gives useful information about the correlation scale of the field; the associated energy power spectrum, whose power-law scaling exponent has to be compared with Kolmogorov-like spectrum observed at MHD scales, while a steeper power law is suggested below proton scales; the Probability Distribution Functions (PDFs) of the scale-dependent increments, whose deviation

from Gaussian will qualitatively illustrate the presence of intermittency, and finally the kurtosis with its scaling exponent.

3.1. Magnetic Field Spectral Properties

Figure 2 shows examples of the autocorrelation function versus time scale, for two different samples of the whole collection, one chosen among the mixed status (E2) and the other one among the weakly-mixed status (O). The behaviour of the autocorrelation function is typical of turbulent fields, i.e., with roughly parabolic shape near the origin, indicating the field smoothness in the "dissipative" range, followed by a slower decay to zero, indicative of the inertial range of turbulence [40]. For the example of Figure 2, the values of the time-scale at which the autocorrelation function approaches zero, are the following. Event E2: $\tau_{corr}(x) = (33 \pm 0.2)s$, $\tau_{corr}(y) = (23 \pm 0.2)s$, $\tau_{corr}(z) = (30 \pm 0.2)s$; Event O: $\tau_{corr}(x) = (42 \pm 0.2)s$, $\tau_{corr}(y) = (32 \pm 0.2)s$, $\tau_{corr}(z) = (47 \pm 0.2)s$.
The values obtained for the three magnetic field components for all the intervals under study vary between 13 s and 58 s, in agreement with the typical values in this region [35,41].
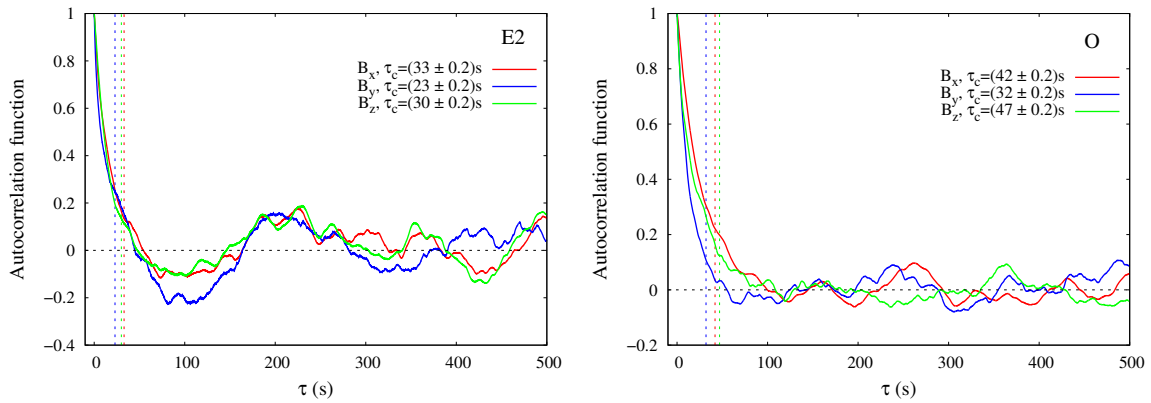

Figure 2. The autocorrelation function for three component of magnetic field, related to the event E2 in the left panel and the event O at the right.

The magnetic energy power spectra provide information about the scaling properties of the field fluctuations. Two examples are given in Figure 3 where we show two characteristic frequencies: the frequency related to the correlation time $f_{corr} = 1/\tau_{corr}$ and the frequency f_{d_i}, related to the ion inertial length of a thermal ion $d_i = c/\omega_{pi}$, i.e., the ratio between light speed and ion plasma frequency. The latter has been estimated assuming the validity of the argument given by Stawarz et al. [35].

Specifically, using the Taylor approximation of relation $\omega_{sc} \simeq \mathbf{k} \cdot \mathbf{v_{ms}}$ and replacing the angular frequency ω with the spatial frequency $f \rightarrow \omega = 2\pi f$, we obtain $2\pi f \simeq k v_{ms}$, and being the wave vector $k = 1/\ell$ the inverse of a typical length (in this work, we use $\ell \sim d_i$), we have: $2\pi f \simeq \frac{v_{ms}}{d_i} \rightarrow f \simeq \frac{v_{ms}}{2\pi d_i}$. At large scales, the correlation frequency very well represents the large-scale boundary of the spectral inertial range. Similarly, the inertial range clearly breaks around the frequency associated with the ion inertial scale f_{d_i}, where kinetic plasma effects start being non-negligible, and in agreement with the usual observations of solar-wind and magnetosheath turbulence [42].

In the MHD range of scales, i.e., above the ion inertial length, the spectrum is well represented by a power law. We report even for the spectra, the measurements of the two selected events, E2 chosen among the mixed status and O for the weakly-mixed status. For the example, in the left panel of Figure 3, we obtain a scaling exponent ~ -1.69, while, for the right panel ~ -1.67. Both values are close to the Kolmogorov value $-5/3$. The average exponent for the three magnetic field component PSDs for all the intervals is $\alpha_{kol} = -1.64 \pm 0.08$, where the error is the standard deviation. Below the typical proton scales, the spectrum is compatible with a steeper power law with exponent which we find, for the examples presented in Figure 3, to be -2.57 for the B_x component in sample E2, and -2.60

for the B_z component in sample O. The exponents found for all components and all intervals lie in the range between -1.89 and -2.76, with a mean value $\alpha_{ion} = -2.44 \pm 0.19$.
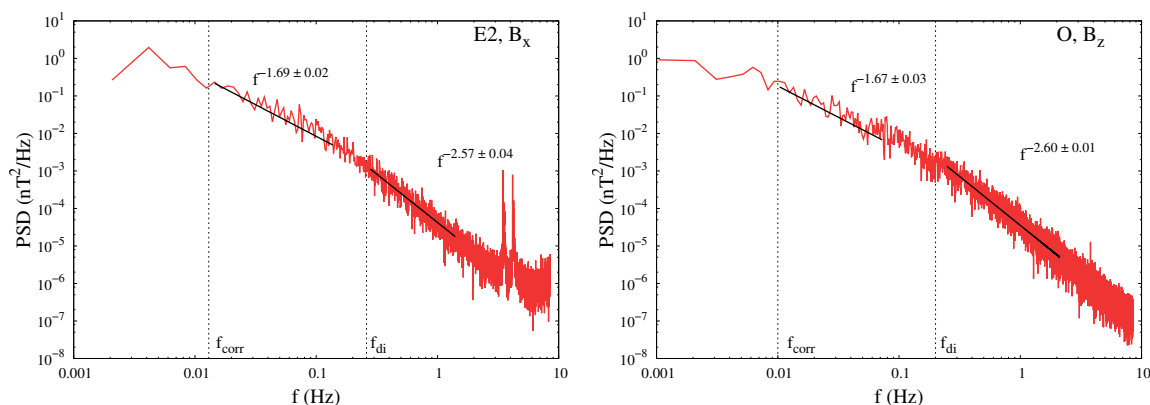

Figure 3. Two examples of the one-dimensional power spectral density (PSD) of the magnetic field. We show here the PSD of B_x for the dataset E2 (left panel) and of B_z for the dataset O (right panel). A Kolmogorov-like spectrum is observed at the MHD scale, while a steeper power law is suggested below ion scales. The vertical black dashed lines indicate the frequency f_{di} related to the ion inertial length d_i, and the frequency related to the correlation time f_{corr}.

The observed spectra seem to indicate that the typical behaviour of space plasma is retrieved in these samples, and that the turbulence might be developing as a consequence of, or superimposed to, the Kelvin–Helmholtz instability. Figure 4 shows how the spectral exponent α_{kol} and the exponent α_{ion} are distributed around the typical expected values.
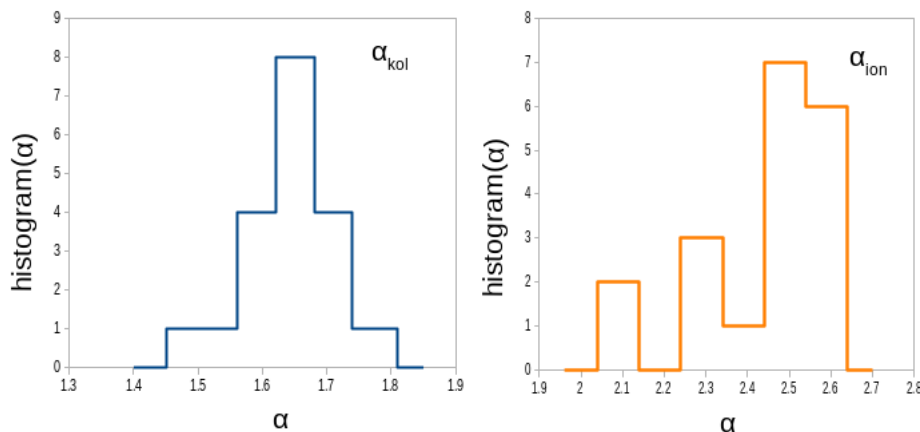

Figure 4. Histograms of the total number of events with the spectral exponent α_{kol}, distributed around the Kolmogorov value 5/3 and the exponent α_{ion}, distributed around the value 2.44. The exponents refer to all three components of the field.

The histograms, collecting the exponents for all magnetic components and for all events, show clearly that the inertial range exponent distribution is sharply peaked around the expected Kolmogorov value $\alpha_{kol} \simeq -5/3$. On the contrary, and in agreement with solar wind observations [43], the small-scale exponents are more broadly distributed around their mean $\alpha_{ion} \simeq 2.44$.

3.2. Intermittency

The statistical properties of turbulent fields cannot be fully described by spectra, and the intermittency in particular requires a more accurate statistical treatment of the fluctuations. For this

reason, we have estimated the PDF for all components of the magnetic field increments at different scales, for all samples here considered. For each scale, the magnetic field increments were standardized by normalizing to their standard deviation to allow the comparison between the different scales. PDFs were thus computed as histograms normalized to the total number of field increments and to the equally spaced bin size, so that the integral of the whole PDF is one. Figure 5 shows two examples of the increment PDFs at five different scales, for the same two intervals and components already shown in previous figures. The black dashed line represents a reference Gaussian distribution. The probability distribution functions are characterized by the increasing deviation from Gaussian towards smaller scales [44–46], typical of intermittent turbulence. At small scales, the distributions show heavy tails indicating the presence of particularly intense magnetic field fluctuations, usually related to the presence of intermittent structures. Similar results were found for all intervals and for all magnetic field components.
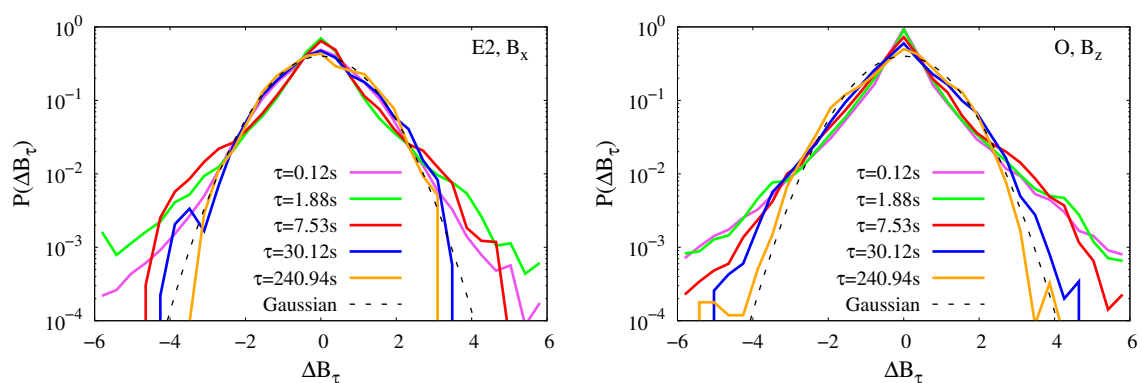

Figure 5. Probability distribution functions of the normalized increments $\Delta B_\tau^{(x)}$ are shown in the left panel for sample E2 and in the right panel for sample O. The black dashed line is a Gaussian distribution used as reference.

A way to quantify the deviation from a Gaussian distribution is the normalized fourth-order moment of the increments, the kurtosis K. In all the intervals under study, the kurtosis of all magnetic field components has the typical Gaussian value $K = 3$ at large scales, roughly down to the correlation scale, and then increases toward small scales as a power law $K(l) \sim l^\kappa$. For all cases, the power-law fitting range was approximately located between the correlation time (at large time scales) and the time associated with the ion-inertial scale, via the Taylor hypothesis (at small time scale). This range is mostly consistent with the observed spectral inertial range, although in some occasions a small shift towards small scales is present. The scaling exponent κ gives a quantitative estimate of the intermittency, i.e., of the anomalous scaling of the magnetic fluctuations [47].

In Navier–Stokes turbulence, it is often observed that $\kappa \simeq 0.1$ [48]. In Figure 6, the scaling exponent of kurtosis is larger, consistent with a more efficient intermittency, for both datasets E2 and O.

Note that at small scales a saturation and decrease of the kurtosis is observed in about half of the cases, as shown in Figure 6 for the E2 event on the left side. For the other cases, the kurtosis keeps its increasing trend or shows a saturation (Figure 6 event O on the right side). The first behaviour, i.e., a saturation and decrease at small scales, is typical of the solar-wind magnetic fluctuations, while it was not usually observed in the magnetosheath (e.g., [35,49]). Although we can exclude instrumental noise effects (the observed scales are sufficiently far from the noise level, as also seen from the spectra), the reason for this behaviour is not fully understood, and it is outside of the scope of the present paper.
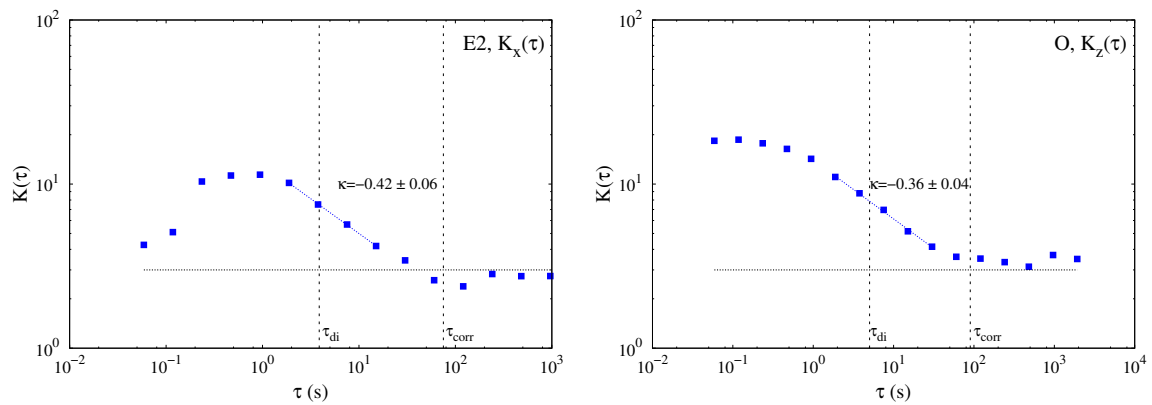
Figure 6. The scaling dependence of the kurtosis *K* for two samples, E2 on the left and O on the right. The Gaussian value $K = 3$ is indicated, as well as power-law fit in the inertial range for the two cases. The vertical black dashed lines indicate the inertial period τ_{di} related to the frequency f_{di}, and the correlation time τ_{corr}.

4. Evolution of the Turbulence along the Flank Magnetopause

Following the analysis of the properties of turbulence in each individual event, we now focus on the possibility to identify signatures of its evolution along the flank magnetopause by comparing the different samples under study. The position along the magnetopause likely corresponds to different stages of the KH evolution, whose possible influence on the turbulence characteristics will be discussed. Turbulence in the dayside magnetopause region is usually strong, and can have several sources besides the KHI [50,51]. These include for example magnetic reconnection poleward of the cusp [16,17,52–56], or kinetic Alfvén waves mode converted in the non-uniform magnetopause region from compressional fluctuations present in the dayside magnetosheath [36,37]. The turbulence observed in our sample could thus be either generated by the identified KHI, or pre-existent, due to other drivers, and modulated by the KHI.

We are interested in understanding if the statistical properties of the field fluctuations, which may be used as an indicator of the state of turbulence, evolve following the development of the KHI along the magnetopause. The majority of the intervals selected for this work were identified as collected in the mixing region of the KHI. This makes our database roughly homogeneous in terms of the macroscopic KHI geometry and of the spacecraft position within the instability structures in the shear direction (approximately corresponding to X in our reference frame). The upstream wind conditions were relatively similar for most of the intervals, as specified in Table A1 in Appendix A. Furthermore, all samples present comparable roll-up period of 2–4 minutes. Using the tailward flow speed listed in Table 1 to transform the period in wavelength, the resulting average KH wavelength is $\sim 6.4\ R_E$, consistent with that reported in the literature [6,12,13,15,23]. In this approximation, the different intervals are thus samples of turbulence at different distances from the instability region, along KHI structures of comparable scale, allowing to study the modulation of turbulence caused by the instability.

Therefore, we will show the variation of the turbulence and intermittency parameters estimated in previous sections as a function of the spacecraft position in the magnetosheath. In Figure 7, the z-component magnetic field correlation scale τ (top left), the fitted spectral power-law index $\alpha_{kol}^{(z)}$ of the z magnetic field component (in the Kolmogorov inertial range) (top right), the spectral index $\alpha_{ion}^{(z)}$ (in the sub-ion range, i.e., for scales smaller than the typical ion scales) (bottom left), and the kurtosis scaling exponent κ are plotted as a function of the -X coordinate. The figure suggests a possible fluctuating behaviour of the parameters as the spacecraft position spans the X-coordinate, visible as a quasi-periodic modulation of the spectral exponents. Although such behaviour does not fit a periodic

function, the approximate wavelength associated with such oscillation can be roughly estimated as $\sim 6 - 7 \, R_E$.

The amplitude of such modulation seems to decrease as the measurements are taken further away from the dusk-dawn line, and for $X \lesssim -15 \, R_E$ the parameters seem to become more stabilized. Note that the fluctuations of the power-law index are typically larger than the estimated fitting error on each value (as clearly visible from the figures).
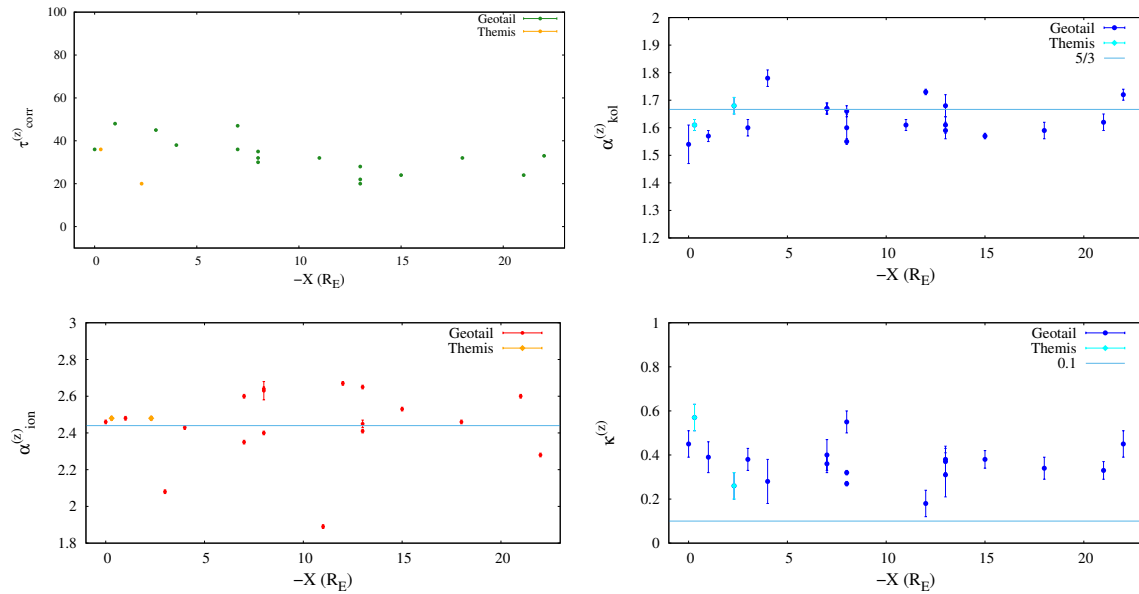

Figure 7. The correlation scale of the component B_z (left-top panel), the fitted power-law index (component z of magnetic field), at MHD scales (right-top panel) and below ion scale of energy spectra (left-bottom panel), as a function of -X coordinate. The value expected for a Kolmogorov-like spectrum is –5/3 that corresponds to the horizontal green line in the top panel. The small-scale reference value is -2.44 [43,57–59]. A modulation is suggested, during the departure along -X coordinate, consistently because the error that affect measures are significantly smaller than the α-index values. In the right-bottom panel, the fitted power-law index of the kurtosis is plotted as a function of -X coordinate. The reference value is $\kappa = 0.101$, which is typical value observed in Navier–Stokes turbulence [48].

This result suggests that, for the observed KHI events, the vortex roll-up periodicity provides a modulation of the associated turbulence at all times, possibly due to the quasi-periodic alternation of dominating plasma (i.e., on both sides of the KHI interface) along the flanks. Eventually, turbulence converges towards a fully developed state, i.e., with a stabilized spectral index, after about $\sim 15 \, R_E$, where the two regions are finally mixed. Note that this type of evolution was also recently observed in numerical simulations of turbulence in the KHI [60].

This interpretation is corroborated by the fact that the observed modulation is persistent for most of the parameters obtained in this analysis. Indeed, the scaling exponent of kurtosis $\kappa^{(z)}$, also shown in the bottom panel of Figure 7, also presents the same modulation, with similar periodicity. For a more comprehensive overview of our observation, the fitted power-law indexes α_{kol}, α_{ion} and the kurtosis scaling index κ are plotted together as a function of the -X, Y, Z coordinate (Figure 8), in order to better visualize the overall behavior which characterizes the KH vortices.
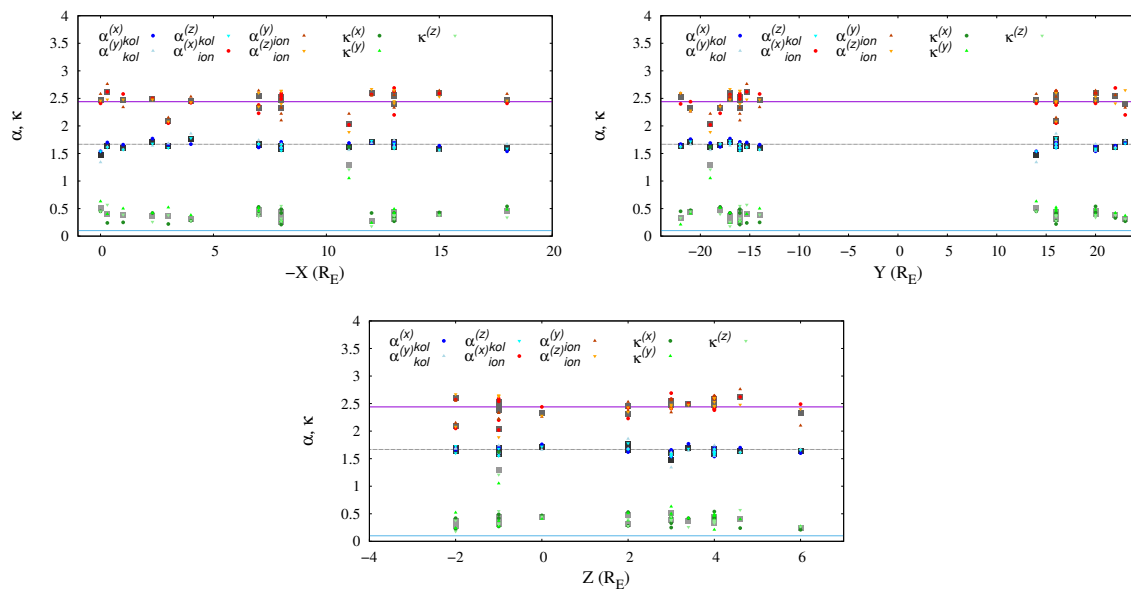
Figure 8. All fitted power-law index, i.e., α_{kolm} at MHD scales (blue symbols), α_{ion} at ion scales (red symbols) and κ scaling exponent of the kurtosis (green symbols), as a function of -*X*, *Y*, *Z* coordinate. Different shades of color and symbol shape refer to the different component (see legend). The mean value of each sample is reported as grey or black square. The overall fluctuating behaviour is seen for all three indexes.

The spectral index α_{kol} at MHD scales is indicated by different shades of blue symbols for his three field components; similarly, α_{ion} is described by different red symbols for the three component, and the index κ of the kurtosis is indicated by green symbols. We have also plotted the mean of three component for each sample as grey squares. Moreover, reference lines at $5/3$, -2.44 and 0.101 are plotted for each exponent, respectively. The fluctuating behaviour is seen for all three indexes. This confirms the possible signature of transition to turbulence in the region downstream of the KH instability, with spectral and intermittency properties evolving while the KHI vortices roll-up. This interpretation requires the assumption that all KHI events studied here might be originated at the same distance from the dusk–dawn line, e.g., at magnetosphere nose, and that the development of the KHI under similar conditions is characterized by a similar evolution of turbulence.

It is noteworthy that the emergence of a clear anti-correlation between the κ and the two spectral indexes, although it is more evident between κ and α_{kol}. In order to look for correlations between the variations in the turbulence parameters, we directly compare the fluctuations around their means of the inertial range spectral exponent and of the kurtosis scaling exponent, as shown in Figure 9 as a function of -*X* for the *z*-component of the field. There is a hint of some correlation in the trend of the two indexes.

To quantitatively measure the amount of such correlations between all parameters, we computed the (linear) Pearson and (rank) Spearman correlation coefficients (respectively, C_P and C_S) for all pairs of turbulent indexes. As also visualized in the scatter plots in Figure 10, the most correlated parameters are $\alpha_{kol}^{(z)}$ and $\kappa^{(z)}$ (left panel at the top), $\alpha_{ion}^{(z)}$ and $\kappa^{(z)}$ (right panel at the top), and the mean magnetosheath speed v_{ms} vs κ (left bottom panel). The correlation timescale τ also is moderately correlated with the kurtosis scaling exponent for the *z*-component of the magnetic field (right bottom panel), while no significant correlation is observed with the other parameters. The presence of correlations, although moderate, strengthens the observation of the spatial structure along the KHI. The bulk plasma velocity correlation with the kurtosis scaling exponent could suggest a role of the velocity in modulating the turbulence. However, no correlation is observed with the spectral exponents, so that this possibility should be disregarded.
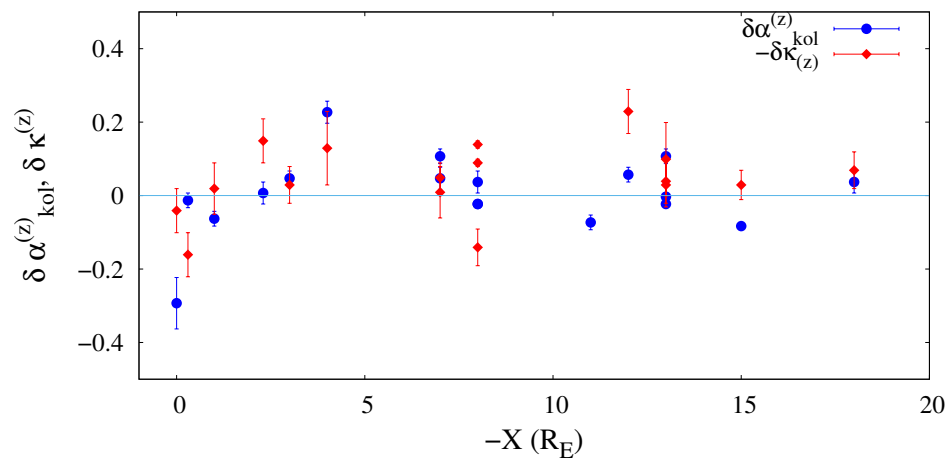
Figure 9. The fluctuation of the fitted power-law index for component z of energy spectra at MHD scales, i.e., α_{kolm} (blue dots) and the fluctuation of the power-law index for component z of the scaling exponent κ of the kurtosis (red dots) as a function of -X coordinate.
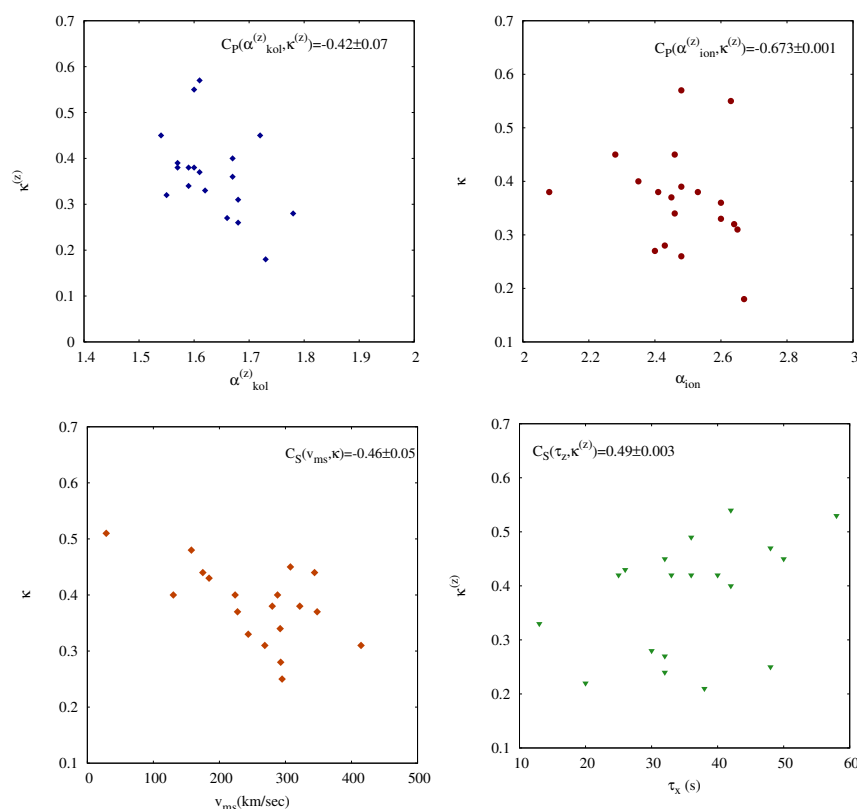

Figure 10. Top left panel: the *z*-component of the scaling exponent κ as a function of the same component of the scaling exponent α_{kol}. Top right panel: the *z*-component of the scaling exponent κ as a function of the same component of the scaling exponent α_{ion}. Bottom left panel: the *x*-component of the scaling exponent κ as a function of the same component of the velocity field. Bottom right panel: the *z*-component of the scaling exponent κ as a function of the magnetic field correlation timescale τ. For each pair of parameters, the largest correlation coefficients, Pearson's (C_P) or Spearman's (C_S), is indicated in the corresponding panel.

5. Conclusions

We have studied and characterized the properties of plasma turbulence and intermittency, along the tail-flank magnetopause and its boundary layer, when Kelvin–Helmholtz instability was reported. We have surveyed the Geotail and THEMIS data, recognized as rolled-up vortices by Fairfield et al. [12], Hasegawa et al. [15], Fairfield et al. [21], Fujimoto et al. [28], Stenuit et al. [29], Lin et al. [30], taken during satellite magnetopause crossings. Firstly, we have applied time-series analysis techniques to the collection of 20 samples, in order to obtain the autocorrelation function, the power spectrum, the probability distribution functions of the field increments and their kurtosis. The behaviour of the autocorrelation functions is standard, with values of the correlation scales τ_{corr} that vary between 13 and 58 s, in agreement with typical values observed in this region. In the MHD range of scales, the spectrum is well represented by a power law with exponent ~ -1.69, not far from the Kolmogorov value $-5/3$. Below the typical proton scales, the spectrum is instead compatible with a steeper power law with exponent which we find in the range between -1.89 and -2.76, with a mean value $\alpha_{ion} = -2.44$. The inertial range clearly breaks around the frequency associated with the ion inertial scale f_{d_i}, where kinetic plasma effects start being non-negligible, and in agreement with the usual observation of solar-wind and magnetosheath turbulence [42]. Probability distribution functions are characterized by high tails and the deviation from Gaussian increases towards smaller scales [44–46]. The fat tails are due to particularly intense magnetic field fluctuations, usually related to the presence of structures. Finally, we have analysed the behaviour of the kurtosis. The range of scales where we showed the presence of a power-law is generally consistent with the spectral inertial range, and the scaling exponent κ gives a quantitative estimate of the intermittency [47]. In light of the results obtained, we have investigated the behaviour of several parameters as a function of the progressive departure along the Geocentric Solar Magnetosphere coordinates, which roughly represent the direction in which we expect the KHI vortices to evolve towards fully developed turbulence. It appears that a fluctuating behaviour of the parameters exist, visible as a decreasing, quasi-periodic modulation with an associated periodicity, estimated to correspond to approximately 6.4 R_E. Such observed wavelength is consistent with the estimated vortices roll-up wavelength reported in the literature for these events [6,12,13,15,23]. The observed modulation seems robust, as it exists for most of the parameters considered in this analysis, which also present moderate correlations among each other. If the turbulence is pre-existent, it is possible that the KHI modulates its properties along the magnetosheath, as we observed.

On the other hand, if we assume that the KHI has been initiated near the magnetospheric nose and develops along the flanks, then the different intervals we study may be sampling the plasma at different stages of evolution of the KH-generated turbulence, after the instability has injected energy in a cascading process as large-scale structures.

Of course, a possible role of the KH boundaries (i.e., of the actual mixing conditions) cannot be excluded, although in that case more random fluctuations of the parameters would be expected. Instead, the presence of a modulation suggests that the KHI events are initiated at the nose, and their structure is relatively similar for all the events studied here. The initial injection scale is persistent as the scale of the modulation of the transition to turbulence. The evolving nature of turbulence is represented by the initially broad, then decreasing fluctuations of the spectral and intermittency indexes. Such regime could be associated with the transient competition between linear dynamics and the emergence of secondary instabilities, which later evolves to fully developed turbulence. In our sample, the observed parameters roughly converge to the typical values of fully developed turbulence at a distance $\sim -15 R_E$ from the dusk–dawn line, corresponding to a factor of 2–3 in terms of the KHI vortex roll-up. This observation might be an indication of the typical distance for the observation of fully developed turbulence initiated by a KH instability. If this behaviour is general, it could be of relevance for KHI near interplanetary shocks, in the solar corona, and in the magnetotail, providing useful information for currently operating and future space missions, such as MMS, the Parker Solar Probe and Solar Orbiter.

Appendix A. Additional Information about Daily Conditions of the Upstream Solar Wind

By using the OMNI database provided by NASA (see the internet address https://omniweb.gsfc.nasa.gov), we have checked the solar wind (SW) conditions relative to the intervals used for each event described. The daily conditions are listed in Table A1, collecting the magnetic field magnitude $|B_{sw}|$ and components, the average values of bulk speed $|V_{sw}|$ and velocity components, the density n_{sw} and temperature T_{sw}. Conditions are generally similar in terms of bulk speed, with some differences in field magnitude and temperature. However, we have checked that these are basically uncorrelated with the turbulence parameters, with correlation coefficients $\lesssim 0.1$.

Table A1. Event List of rolled-up vortices detected by Geotail over nine years from 1995 to 2003, adapted from Hasegawa et al. [15]. The last two events were detected by THEMIS probe C, adapted by Lin et al. [30]. We collected the daily conditions of solar wind: the magnetic field magnitude $|B_{sw}|$, the mean values of three components of the field B_x^{sw}, B_y^{sw}, B_z^{sw}, the average values of bulk speed $|V_{sw}|$, the mean values of three components of the velocity V_x^{sw}, V_y^{sw}, V_z^{sw}, the values of the proton density n_{sw} and proton temperature T_{sw}.

Event	Interval (UT)	$|B_{sw}|$ (nT)	B_x^{sw}, B_y^{sw}, B_z^{sw} (nT)	$|V_{sw}|$ (km/s)	V_x^{sw}, V_y^{sw}, V_z^{sw} (km/s)	n_{sw} (1/cm³)	T_{sw} (K)
			Geotail Mission				
S	1995-03-24 0600-0800	9.7	1.4; −4.5; 8.3	332	−332; 12.3; −6,3	18.1	18,018
O	1997-01-10 2050-2400	13.7	−2.5; −11.8; 5.7	414	−414; 3.4; −13.9	20.6	11,343
P	1997-01-11 0400-0500	22.2	−7.5; −3.8; 20.3	454	−453; −19.0; 16.0	14.1	116,348
Q	1997-02-12 1430-1600	3.5	−0.7; −0.3; 3.3	382	−382; −4.1; −2.5	5.4	22,156
T	1998-04-13 0315-0430	8.8	4.5; −2.9; 6.7	390	−390; −5.5; 4.8	3.8	23,776
L	1998-08-01 0530-0730	9.7	−2.6; 7.8; 8.9	404	−404; −7.9; −8.2	8.3	35,023
D	1998-12-27 1800-2100	5.2	−1.8; 6.2; 4.7	371	−370; −10.1; −29.3	4.4	34,764
N	1999-02-15 1445-1515	8.2	−2.0; 3.9; 5.2	600	−599; 25.5; −8.0	3.7	187,717
M	1999-07-20 0630-0730	6.3	−2.1; 0.2; 5.9	303	−303; 3.2; −5.0	15.4	25,486
E	2000-11-01 1030-1200	6.6	4.5; −0.2; 4.5	443	−443; −8.7; −11.6	6.2	86,515
H	2001-01-25 1330-1630	3.4	1.5; −1.7; 1.8	372	−372; 10.4; −13.1	4.5	10,762
B	2001-11-16 1900-2000	8.9	−3.6; 5.4; 2.9	379	−378; 1.6; −14.5	4.0	59,474
C	2001-12-07 2000-2130	5.4	2.3; −2.0; 3.4	462	−461; 19.3; 9.1	3.1	101,406
E2	2002-03-25 0530-0900	17.0	5.7; −13.1; 9.0	444	−443; 6.5; 17.9	5.7	37,541
F	2002-03-25 1000-1300	14.8	5.2; −11.0; 8.2	435	−435; −9.2; 12.1	6.7	20,890
A	2002-10-15 2100-2300	14.9	2.7; 8.6; 5.5	532	−525; 49.8; −61.1	4.1	812,629
R	2003-07-17 0330-0500	3.9	2.7; −1.3; 1.8	632	−632; 11.5; 13.5	2.6	190,142
			THEMIS Mission				
TH1	2008-11-06 0850-0920	2.7	2.1; −0.8; 1.5	288	−288; −8.7; 3.1	6.5	14,542
TH2	2008-11-18 0720-0730	3.4	-0.9; −1.1; 3.1	347	−346; −15.1; 9.9	4.5	31,423

References

1. Pucci, F.; Malara, F.; Perri, S.; Zimbardo, G.; Sorriso-Valvo, L.; Valentini, F. Energetic particle transport in the presence of magnetic turbulence: influence of spectral extension and intermittency. *Mon. Not. R. Astron. Soc.* **2016**, *459*, 3395–3406. [CrossRef]

2. Zimbardo, G.; Greco, A.; Veltri, P.; Voros, Z.; Taktakishvili, A.L. Magnetic turbulence in and around the Earth's magnetosphere. *Astrophys. Space Sci. Trans.* **2008**, *4*, 35–40. [CrossRef]

3. Mitchell, D.G.; Kutchko, F.; Williams, D.J.; Eastman, T.E.; Frank, L.A.; Russell, C.T. An extended study of the low-latitude boundary layer on the dawn and dusk flanks of the magnetosphere. *J. Geophys. Res.* **1987**, *92*, 7394–7404. [CrossRef]

4. Bavassano Cattaneo, M.B.; Marcucci, M.F.; Bogdanova, Y.V.; Rème, H.; Dandouras, I.; Kistler, L.M.; Lucek, E. Global reconnection topology as inferred from plasma observations inside Kelvin–Helmholtz vortices. *Ann. Geophys.* **2010**, *28*, 893–906. [CrossRef]

5. Johnson, J.R.; Wing, S.; Delamere, P.A. Kelvin Helmholtz Instability in Planetary Magnetospheres. *Space Sci. Rev.* **2014**, 184, 1–31. [CrossRef]

6. Hasegawa, H. Comment on "Evolution of Kelvin–Helmholtz activity on the dusk flank magnetopause" by Foullon et al. *J. Geophys. Res.* **2009**, *114*, A03205. [CrossRef]

7. Sckopke, N.; Paschmann, G.; Haerendel, G.; Sonnerup, B.U.; Bame, S.J.; Forbes, T.G.; Hones, E.W.; Russell, C.T. Structure of the low-latitude boundary layer. *J. Geophys. Res.* **1981**, *86*, 2099–2110. [CrossRef]

8. Sonnerup, B. Theory of the low-latitude boundary layer. *J. Geophys. Res.* **1980**, *85*, 2017–2026. [CrossRef]

9. Lui, A.T.Y.; Venkatesan, D.; Murphree, J.S. Auroral bright spots on the dayside oval. *J. Geophys. Res.* **1989**, *94*, 5515. [CrossRef]

10. Yamamoto, T. A linear analysis of the hybrid Kelvin-Helmholtz/Rayleigh-Taylor instability in an electrostatic magnetosphere-ionosphere coupling system. *J. Geophys. Res.* **2008**, *113*, A06206. [CrossRef]

11. Chen, S.H.; Kivelson, M.G. On nonsinusoidal waves at the Earth's magnetopause. *Geophys. Res. Lett.* **1993**, *20*, 2699–2702. [CrossRef]

12. Fairfield, D.H.; Otto, A.; Mukai, T.; Kokubun, S.; Lepping, R.P.; Steinberg, J.T.; Lazarus, A.J.; Yamamoto, T. Geotail observations of the Kelvin–Helmholtz instability at the equatorial magnetotail boundary for parallel northward fields. *J. Geophys. Res.* **2000**, *105*, 21159–21173. [CrossRef]

13. Kivelson, M.G.; Chen, S.H. *The Magnetopause: Surface Waves and Instabilities and Their Possible Dynamical Consequences*; Geophys. Monogr. Ser., 90; Song, P., Sonnerup, B.U.Ö., Thomsen, M.F.; , Eds. American Geophysicsl Union: Washington, DC, USA, 1995; Volume 20, pp. 257–268.

14. Fujimoto, M.; Tonooka, T.; Mukai, T. *Vortex-Like Fluctuations in the Magnetotail Flanks and Their Possible Roles in Plasma Transport*; Geophys. Monogr. Ser. 133; Newell, P.T., Onsager, T., Eds.; American Geophysicsl Union: Washington, DC, USA, 2003; pp. 241–251.

15. Hasegawa, H.; Fujimoto, M.; Takagi, K.; Saito, Y.; Mukai, T.; Rème, H. Single-spacecraft detection of rolled-up Kelvin–Helmholtz vortices at the flank magnetopause. *J. Geophys. Res.* **2006**, *111*, A09203.

16. Terasawa, T.; Fujimoto, M.; Mukai, T.; Shinohara, I.; Saito, Y.; Yamamoto, T.; Machida, S.; Kokubun, S.; Lazarus, A.J.; Steinberg, J.T.; et al. Solar wind control of density and temperature in the near-Earth plasma sheet: Wind/Geotail collaboration. *Geophys. Res. Lett.* **1997**, *24*, 935–938. [CrossRef]

17. Wing, S.; Newell, P.T. 2D plasma sheet ion density and temperature profiles for northward and southward IMF. *Geophys. Res. Lett.* **2002**, *29*, 9. [CrossRef]

18. Sundberg, T.; Boardsen, S.A.; Slavin, J.A.; Anderson, B.J.; Korth, H.; Zurbuchen, T.H.; Raines, J.M.; Solomon, S.C. MESSENGER orbital observations of large-amplitude Kelvin-Helmholtz waves at Mercury's magnetopause. *J. Geophys. Res.* **2012**, *117*, A04216. [CrossRef]

19. Nakamura, T.K.M.; Hasegawa, H.; Daughton, W.; Eriksson, S.; Li, W.Y.; Nakamura, R. Turbulent mass transfer caused by vortex induced reconnection in collisionless magnetospheric plasmas. *Nat. Commun.* **2017**, *8*, 1582. [CrossRef] [PubMed]

20. Chen, S.H.; Kivelson, M.G.; Gosling, J.T.; Walker, R.J.; Lazarus, A.J. Anomalous aspects of magnetosheath flow and of the shape and oscillations of the magnetopause during an interval of strongly northward interplanetary magnetic field. *J. Geophys. Res.* **1993**, *98*, 5727–5742. [CrossRef]

21. Fairfield, D.H.; Kuznetsova, M.M.; Mukai, T.; Nagai, T.; Gombosi, T.I.; Ridley, A.J. Waves on the dusk flank boundary layer during very northward interplanetary magnetic field conditions: Observations and simulation. *J. Geophys. Res.* **2007**, *112*, A08206. [CrossRef]

22. Farrugia, C.J.; Gratton, F.T.; Torbert, R.B. Viscous-type processes in the solar wind-magnetosphere interaction, *Space Sci. Rev.* **2001**, *95*, 443–456.

23. Hasegawa, H.; Fujimoto, M.; Phan, T.D.; Rème, H.; Balogh, A.; Dunlop, M.W.; Hashimoto, C.; Tandokoro, R. Transport of solar wind into Earth's magnetosphere through rolled-up Kelvin–Helmholtz vortices. *Nature* **2004**, *430*, 755–758. [CrossRef] [PubMed]

24. Kokubun, S.; Yamamoto, T.; Acuna, M.H.; Hayashi, K.; Shiokawa, K.; Kawano, H. The GEOTAIL magnetic field experiment. *J. Geomag. Geo-Electr.* **1994**, *46*, 7–21. [CrossRef]

25. Otto, A.; Fairfield, D.H. Kelvin-Helmholtz instability at the magnetotail boundary: MHD simulation and comparison with Geotail observations. *J. Geophys. Res.* **2000**, *105*, 17521. [CrossRef]

26. Foullon, C.; Farrugia, C.J.; Fazakerley, A.N.; Owen, C.J.; Gratton, F.T.; Torbert, R.B. Evolution of Kelvin-Helmholtz activity on the dusk flank magnetopause. *J. Geophys. Res.* **2008**, *113*, A11203. [CrossRef]

27. Fairfield, D.H.; Farrugia, C.J.; Mukai, T.; Nagai, T.; Federov, A. Motion of the dusk flank boundary layer caused by solar wind pressure changes and the Kelvin-Helmholtz instability: 10–11 January 1997. *J. Geophys. Res.* **2003**, *108*, 1460–1471. [CrossRef]

28. Fujimoto, M.; Terasawa, T.; Mukai, T. *The Low-Latitude Boundary Layer in the Tail-Flanks*; Geophysical Monograph 105; Nishida, A., Baker, D.N., Cowley, S.W.H., Eds.; American Geophysical Union: Washington, DC, USA, 1998; pp. 33–44.

29. Stenuit, H.; Fujimoto, M.; Fuselier, S.A.; Sauvaud, J.A.; Wing, S.; Fedorov, A.; Budnik, E.; Savin, S.P.; Trattner, K.J.; Angelopoulos, V.; et al. Multispacecraft study on the dynamics of the dusk-flankmagnetosphere under northward IMF: 10–11 January 1997. *J. Geophys. Res.* **2002**, *107*, 1333. [CrossRef]

30. Lin, D.; Wang, C.; Li, W.; Tang, B.; Guo, X.; Peng, Z. Properties of Kelvin–Helmholtz waves at the magnetopause under northward interplanetary magnetic field: Statistical study. *J. Geophys. Res.* **2014**, *119*, 7485–7494. [CrossRef]

31. Takagi, K.; Hashimoto, C.; Hasegawa, H.; Fujimoto, M.; TanDokoro, R. Kelvin-Helmholtz instability in a magnetotail flank-like geometry: Three-dimensional MHD simulations. *J. Geophys. Res.* **2006**, *111*, A08202. [CrossRef]

32. Taylor G.I. The Spectrum of Turbulence. *Proc. R. Soc. Lond. A* **1938**, *164*, 476–490. [CrossRef]

33. Klein, K.G.; Howes, G.G.; TenBarge, J.M. The violation of the Taylor hypothesis in measurements of solar wind turbulence. *Astrophys. J. Lett.* **2014**, *790*, L20. [CrossRef]

34. Fredricks, R.W.; Coroniti, F.V. Ambiguities in the deduction of rest frame fluctuation spectra from spectra computed in moving frames. *J. Geophys. Res.* **1976**, *81*, 5591–5595. [CrossRef]

35. Stawarz, J.E.; Eriksson, S.; Wilder, F.D.; Ergun, R.E.; Schwartz, S.J.; Pouquet, A.; Burch, J.L.; Giles, B.L.; Khotyaintsev, Y.; Contel, O.L.; et al. Observations of turbulence in a Kelvin–Helmholtz event on 8 September 2015 by the Magnetospheric Multiscale mission. *J. Geophys. Res.* **2016**, *121*, 11021–11034. [CrossRef]

36. Chaston, C.C.; Wilber, M.; Mozer, F.S.; Fujimoto, M.; Goldstein, M.L.; Acuna, M.; Rème, H.; Fazakerley, A. Mode Conversion and Anomalous Transport in Kelvin–Helmholtz Vortices and Kinetic Alfvén Waves at the Earth's Magnetopause. *Phys. Rev. Lett.* **2007**, *99*, 175004. [CrossRef] [PubMed]

37. Chaston, C.C.; Bonnell, J.W.; Clausen, L.; Angelopoulos, V. Energy transport by kinetic-scale electromagnetic waves in fast plasma sheet flows. *J. Geophys. Res.* **2012**, *117*, A09202. [CrossRef]

38. Hapgood, M.A. Space physics coordinate transformations-A user guide. *Planet Space Sci.* **1992**, *40*, 711–717. [CrossRef]

39. Russell, C.T. Geophysical Coordinate Transformations. *Cosmic Electrodyn.* **1971**, *2*, 184–196.

40. Pope, S. *Turbulent Flows*; Cambridge University Press: Cambridge, UK, 2000.

41. Gutynska, O.; Šafránková, J.; Němeček, Z. Correlation length of magnetosheath fluctuations: Cluster statistics. *Ann. Geophys.* **2008**, *26*, 2503–2513. [CrossRef]

42. Leamon, R.J.; Smith, C.W.; Ness, N.F.; Matthaeus, W.H.; Wong, H.K. Observational constraints on the dynamics of the interplanetary magnetic field dissipation range. *J. Geophys. Res.* **1998**, *103*, 4775–4787. [CrossRef]

43. Sahraoui, F.; Belmont, G.; Rezeau, L.; Cornilleau-Wehrlin, N.; Pinçon, J.L.; Balogh, A. Anisotropic Turbulent Spectra in the Terrestrial Magnetosheath as Seen by the Cluster Spacecraft. *Phys. Rev. Lett.* **2006**, *96*, 075002. [CrossRef]

44. Frisch, U. *Turbulence. The Legacy of A. N. Kolmogorov*; Cambridge University Press: Cambridge, UK, 1995.

45. Sorriso-Valvo, L.; Carbone, V.; Veltri, P.; Consolini, G.; Bruno, R. Intermittency in the solar wind turbulence through probability distribution functions of fluctuations. *Geophys. Res. Lett.* **1999**, *26*, 1801–1804. [CrossRef]

46. Bruno, R.; Carbone, V. The Solar Wind as a Turbulence Laboratory. *Living Rev. Sol. Phys.* **2005**, *2*, 4. [CrossRef]

47. Sreenivasan, K.R.; Antonia, R.A. The phenomenology of small-scale turbulence. *Ann. Rev. Fluid Mech.* **1997**, *29*, 435–472. [CrossRef]

48. Anselmet, F.; Gagne, Y.; Hopfinger, E.J.; Antonia, R.A. High-order velocity structure functions in turbulent shear flows. *J. Fluid Mech.* **1984**, *140*, 63–89. [CrossRef]

49. Chhiber, R.; Chasapis, A.; Bandyopadhyay, R.; Parashar, T.N.; Matthaeus, W.H.; Maruca, B.A.; Moore, T.E.; Burch, J.L.; Torbert, R.B.; Russell, C.T.; et al. Higher-order turbulence statistics in the Earth's magnetosheath and the solar wind using Magnetospheric Multiscale observations. *J. Geophys. Res.* **2018**, *123*, 9941–9954. [CrossRef]

50. Book, D.L.; Sibeck, D.G. Plasma transport through the magnetopause turbulent interchange processes. *J. Geophys. Res.* **1995**, *100*, 9567–9573. [CrossRef]

51. Labelle, J.; Treumann, R.A. Plasma waves at the dayside magnetopause. *Space Sci. Rev.* **1988**, *47*, 175–202. [CrossRef]

52. Bavassano Cattaneo, M.B.; Marcucci, M.F.; Retinò, A.; Pallocchia, G.; Rème, H.; Dandouras, I.; Kistler, L.M.; Klecker, B.; Carlson, C.W.; Korth, A.; et al. Kinetic signatures during a quasi-continuous lobe reconnection event: Cluster Ion Spectrometer (CIS) observations. *J. Geophys. Res.* **2006**, *111*, A09212. [CrossRef]

53. Frey, H.U.; Phan, T.D.; Fuselier, S.A.; Mende, S.B. Continuous magnetic reconnection at Earth's magnetopause. *Nature* **2003**, *426*, 533–537. [CrossRef]

54. Phan, T.D.; Dunlop, M.W.; Paschmann, G.; Klecker, B.; Bosqued, J.M.; Rème, H.; Balogh, A.; Twitty, C.; Mozer, F.S.; Carlson, C.W.; et al. Cluster observations of continuous reconnection at the magnetopause under steady interplanetary magnetic field conditions. *Ann. Geophys.* **2004**, *22*, 2355–2367. [CrossRef]

55. Retinò, A.; Bavassano Cattaneo, M.B.; Marcucci, M.F.; Vaivads, A.; André, M.; Khotyaintsev, Y.; Phan, T.; Pallocchia, G.; Rème, H.; Möbius. E.; et al. Cluster multispacecraft observations at the high-latitude duskside magnetopause: Implications for continuous and component magnetic reconnection. *Ann. Geophys.* **2005**, *23*, 461–473.

56. Song, P.; Russell, C.T. A model of the formation of the low-latitude boundary layer. *J. Geophys. Res.* **1992**, *97*, 1411. [CrossRef]

57. Breuillard, H.; Yordanova, E.; Vaivads, A.; Alexandrova, O. The effects of kinetic instabilities on small-scale turbulence in Earth's magnetosheath. *Astrophys. J.* **2016**, *829*, 54–60. [CrossRef]

58. Zimbardo, G.; Greco, A.; Sorriso-Valvo, L.; Perri, S.; Vöros, Z.; Aburjania, G.; Chargazia, K.; Alexandrova, O. Magnetic turbulence in the geospace environment. *Space Sci. Rev.* **2010**, *156*, 89–134. [CrossRef]

59. Alexandrova, O.; Chen, C.H.K.; Sorriso-Valvo, L.; Horbury, T.S.; Bale, S.D. Solar Wind Turbulence and the Role of Ion Instabilities. *Space Sci. Rev.* **2013**, *178*, 101–139. [CrossRef]

60. Rossi, C.; Califano, F.; Retinò, A.; Sorriso-Valvo, L.; Henri, P.; Servidio, S.; Valentini, F.; Chasapis, A.; Rezeau, L. Two-fluid numerical simulations of turbulence inside Kelvin–Helmholtz vortices: Intermittency and reconnecting current sheets. *Phys. Plasmas* **2015**, *22*, 122303. [CrossRef]